Proceedings of the Seventh International Conference on
Railway Technology: Research, Development and Maintenance
Edited by: J. Pombo
Civil-Comp Conferences, Volume 15, Paper 5.13
Civil-Comp Press, Edinburgh, United Kingdom, 2026
ISSN: 2753-3239, doi: 10.4203/ccc.15.5.13
©Civil-Comp Ltd, Edinburgh, UK, 2026

Numerical Analysis of Freight Train-Tunnel Overpressure Through Steady-State CFD Simulations

E. Inghilleri, G. Tomasini, S. Negri and N. Chizzolini

Department of Mechanical Engineering, Politecnico di Milano, Italy

Abstract

Train–tunnel overpressure has been mainly studied for high-speed trains, while limited attention has been given to freight trains. This is mainly due to pressure variations scaling with the square of train velocity, and freight trains generally operating at lower speeds. However, freight trains may still produce significant pressure levels, which during crossings with passenger trains can lead to passenger discomfort and potential infrastructure damage. This work extends the current understanding of freight train–tunnel overpressure by analysing the effects of wagon geometry, train length, and inter-vehicle gaps using a simplified steady-state CFD approach. Results show that wagon geometry affects the pressure signature, both in terms of local pressure peaks and boundary layer development. The effect of inter-vehicle gaps depends on the balance between pressure growth at wagon leading edges and pressure recovery upstream of trailing wagons. For homogeneous trains with a well-developed boundary layer, larger gaps increase pressure peaks by up to 29%, whereas for configurations with large spacing and thicker boundary layers, increasing gaps reduce peak pressures by up to 34%. Train length effects are assessed using a container train with three different lengths, showing an approximately linear pressure increase with convoy length.

Keywords: train aerodynamics, freight trains, train-tunnel overpressure, CFD simulations, wagon geometry, convoy composition

1 Introduction

When a train enters and traverses a tunnel, the transition from open-air conditions to a confined environment gives rise to the phenomenon referred to as overpressure. The entry of the train nose into the tunnel generates a compression wave that propagates through the tunnel at the speed of sound in a piston-like manner. Conversely, the entry of the tail produces a rarefaction wave. Upon reaching the opposite portal, the waves are reflected back in opposite nature. Moreover, as the train travels inside the tunnel, it perturbs the near-field flow due to its motion. Inside the tunnel, the propagation and superposition of these pressure variations form a complex wave system, resulting in transient loads on both the vehicle and the tunnel structure.
The overpressure phenomenon can cause significant damage to infrastructures and negatively affect passenger comfort. Current European standards, namely EN 14067-5 [1] and TSI Infrastructures [2], prescribe the maximum pressure variation generated by the passage of a train in a specific tunnel, thus ensuring acoustic safety and acceptable comfort levels for passengers.
The phenomenon has been studied using various methodologies over the past decades. Experimental tests have been conducted, both at full scale [3,4] and using scaled models [5,6]. These studies allowed validation of several numerical models, including both three-dimensional CFD simulations and simplified one-dimensional approaches.
A wide overview is now available in the literature, covering the effects of train speed, shape, and length [7], as well as the influence of tunnel geometry, length, and blockage ratio [6, 8]. Over the years, even specific aspects of tunnel design, such as the presence of air shafts and their influence on pressure waves, have been investigated [9,10]. Lately, the case of train crossings has also been analyzed [11, 12], revealing that the resulting pressure levels can either worsen or improve depending on the time interval between the trains' entry into the tunnel. However, most of the existing research has focused on passenger rolling stock and in particular on high speed trains, reflecting their higher operating speeds and the associated aerodynamic challenges.
Only in recent years has increasing attention been devoted to freight trains, and the majority of studies on the topic consider the open-air scenario. The aerodynamics of an isolated container was analysed through Large-Eddy Simulations in [13], whereas the aerodynamics of an operational freight train was studied in [14], making use of Detached-Eddy Simulations. [15] investigated the response to crosswind of a high-speed freight train for intermodal transportation through reduced-scale model wind tunnel experiments. Conversely, only a limited number of studies have specifically investigated the overpressure generated by freight trains in tunnels, mainly because pressure increases with the square of the train speed, while freight services typically operate at lower velocities.
To the best of the authors' knowledge, no dedicated full-scale experimental campaigns

focused on freight-train pressure signatures in tunnels are currently available in the literature and the phenomenon has only been studied experimentally using reduced-scale model tests. The first dedicated investigation was carried out in [5] by means of a 1:25 moving-model experimental campaign, where the authors studied the influence of inter-wagon gaps on the generated pressure waves. Owing to the complexity and cost of experimental testing, subsequent research has increasingly relied on numerical approaches.

CFD simulations based on sliding-mesh techniques were first employed in [16] to reproduce the overpressure phenomenon generated by freight trains inside tunnels. Later studies [17, 18] further analysed the separated-flow structures developing around blunt freight-train geometries and exploited CFD results to improve one-dimensional models specifically tailored for freight applications.

The present work aims at extending the investigation of the parameters governing the pressure signature generated by freight trains in tunnels by means of steady-state CFD simulations.

The paper first presents the experimental setup together with the validation of the numerical methodology adopted. The numerical model is then described and employed to investigate the influence of some of the key aerodynamic parameters of freight trains, i.e. wagon geometry, train length and inter-vehicle gaps. Finally, the results are discussed and the main conclusions outlined.

2 Model validation and experimental setup

The numerical model employed for the analysis has been validated against a full-scale experimental campaign conducted on the Italian railway network by Politecnico di Milano. The experimental campaign was carried out in the ”Monte Cellarino” tunnel in 2020. The tunnel is located in Capena, near Rome, and is part of the Direttissima high-speed railway line connecting Florence and Rome. The tunnel is 3177 m long and has a horseshoe-shaped cross-section with an area of $54m^2$. It consists of a double-track configuration with bidirectional traffic and no ballast.

To measure the air velocity inside the tunnel, a GILL WindMaster 3-Axis Ultrasonic Anemometer was placed 300 m from the entrance, on the even-track side, at a height of 2 m. The instrument has a maximum sampling frequency of 32 Hz and a measurement uncertainty of approximately ±0.2 m/s.

For pressure measurements, multiple AMS 4711 barometric sensors were installed at different tunnel sections, on both even and odd track sides, following the EN 14067-5 standard [1]. All sensors were positioned at a height of 1.5 m above the rail level.

An accelerometer was mounted at the midline of the even track to trigger the data acquisition system when the measured acceleration exceeded the predefined threshold of $0.5g$, corresponding to the arrival of a train. The experimental setup is shown in Figure 1. Even though the experimental campaign primarily focused on high-speed trains, a total of 18 freight train passages were identified. Among all the freight train passages, only two present a combination of train length and speed that results in a pressure signal only slightly affected by wave reflections. The two usable datasets correspond to train no. 68364, recorded on October 26th, 2020, and train no. 68380, recorded on November 2nd, 2020.

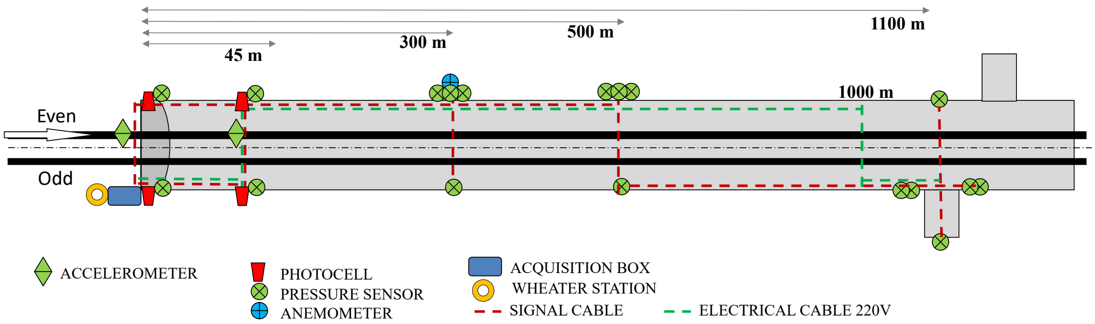

Figure 1: Monte Cellarino tunnel experimental setup.

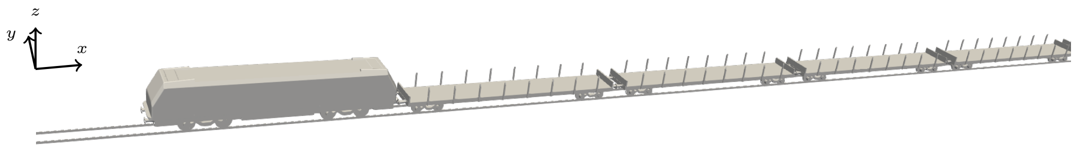

Figure 2: Detail of the train geometry adopted for the numerical-experimental comparison.

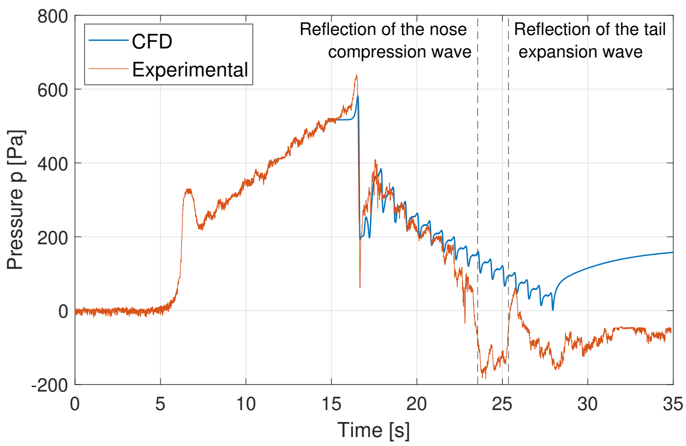

Figure 3: Comparison between experimental and numerical TNS curves.

The train no. 68380 was selected since it presented a uniform convoy configuration whereas the train no. 68364 was composed of wagons of different lengths and

types. The train has a total length of 318 m and it consists of 16 vehicles (an FS E494 locomotive and 15 RGS unloaded wagons). The bogies are the Y25. A detail of the reconstructed train CAD model is shown in Figure 2.
Figure 3 shows the comparison between the experimental and the numerical results. The pressure sensor P120, located on the even side at 300 m from the tunnel entrance is selected for the data comparison. This choice was made to minimize the impact of pressure waves reflection on the signal measured by the sensor. CFD results reproduce the experimental pressure trend with good agreement (i.e. average percentage error below 3%) up to $t = 22s$, where the effects of the reflected compression wave generated by the train head begin to influence the pressure measurements.

3 Numerical setup

The numerical simulations of this work are performed by solving the 3D Reynolds-Averaged Navier–Stokes (RANS) equations coupled with the $k - \omega$ SST turbulence model [19, 20]. The governing equations are discretized using the Finite Volume Method (FVM) with second-order spatial accuracy and solved in OpenFOAM.
The numerical method adopted is the one proposed and validated in [21] for high-speed trains. In particular, the method consists in reconstructing the Train Near-field Signature (TNS) through steady-state simulations of a stationary train inside a tunnel. This approach is based on the assumption that, in the absence of reflected pressure waves, the flow field around the train can be regarded as quasi-steady.
A compressible model has been employed and no relative velocity due to the piston effect was considered.
To reproduce the real domain, a CAD reconstruction of the Monte Cellarino tunnel is carried out using the sectional data provided by RFI. The tunnel geometry is modeled as a smooth, constant-section duct, neglecting surface roughness and wall niches.
The overall length of the computational domain is defined to avoid boundary effects on the flow field: as illustrated in Figure 4a, the inlet section is located 100 m upstream of the train nose, while the outlet is placed 200 m downstream of the train tail. This choice ensures a fully developed flow upstream of the train and a proper wake development downstream. Simulations that feature trains of different lengths conform to the same logic and maintain the same distances between the train and the computational domain boundaries.

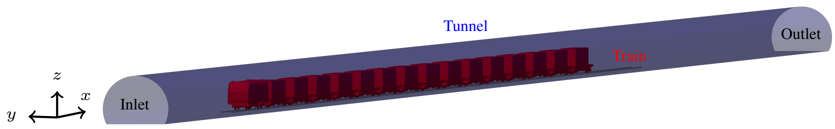

(a) Computational domain.

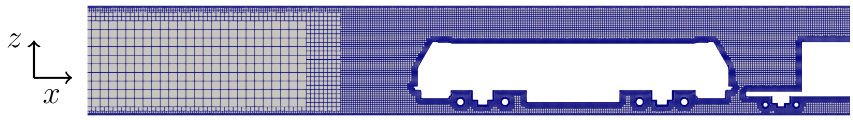

(b) Mesh visualization (front view)

Figure 4: Computational setup and mesh visualization.

The mesh, a detail of which is visible in Figure 4b, has been chosen after a grid independence study, where the effects of the pressure signature have been compared across six different meshes, as shown in Table 1. The selected mesh is the medium without layers, since it provides consistent results (average pressure variation of about 3.8% and maximum relative error of about 7% in the wake pressure recovery) with a computational cost drop of 62% with respect to the fine mesh with layers.
The effect of prismatic layer inflation has been investigated showing only minor effects on the results, while significantly increasing the computational costs of the simulations. As a matter of fact, a freight train can be considered a bluff body where the flow is mainly governed by geometric separation rather than by the development of a well-defined attached boundary layer.

Table 1: Mesh independence: average ($\epsilon_{p,avg}$) and maximum ($\epsilon_{p,max}$) pressure deviations with respect to the reference case (fine grid with layers).

Case	**N. cells**	$\epsilon_{p,avg}$	$\epsilon_{p,max}$
Coarse, no layers	9.8×10^6	12.4%	20%
Coarse, with layers	13.4×10^6	11.4%	18.6%
Medium, no layers	28×10^6	3.8%	7.2%
Medium, with layers	60×10^6	6.2%	9.5%
Fine, no layers	49.4×10^6	-0.3%	7%
Fine, with layers	75.5×10^6	ref	ref

4 Results

This section presents the results of the CFD simulations. It is divided into two subsections, which separately analyze the effects of the investigated parameters, namely wagon geometry and convoy composition.

Figure 5 provides a schematic overview of the investigated train configurations, highlighting the main differences among them. Further details on each case are provided in the following subsections. All results are presented in terms of pressure variations relative to the pressure measured at the train nose.

Figure 5: Lateral view of the trains geometries simulated[1].

4.1 Wagon geometric effects

To investigate the effects of the wagon geometric modifications a set of geometrical configurations representative of typical freight railway operations is considered. The effects of the wagon geometry are isolated considering trains that are homogeneous, fully-loaded and of the same length, i.e. 318 m. The trains employed for this analysis are listed in Table 2 and the resulting TNS curves are shown in Figure 6. The first noteworthy observation can be made comparing *Train 1* and *Train 2*. In this case, the difference in wagon geometry is related to the wagon height that for the High Cube containers, i.e. *Train 2*, is 1 ft higher. The increased exposed area in this configuration leads to a pressure increase at each wagon leading edge.
The direct comparison of the wagon geometric effects between container-type wagons and RILNS-type wagons is possible only between *Train 3* and *Train 4*. This is because RILNS wagons are typically 60 ft long; comparing them with wagons of different lengths would introduce inter-vehicle gap effects, as discussed in the following section. The two configurations exhibit similar pressure levels in the first half of the convoy, whereas the curves diverge after approximately 200 m along the train, showing an increase of more than 30% in the negative peak pressure for *Train 4*. In the

[1] Train 7 and Train 8 are not reported in this figure since they share the same characteristics as Train 1, differing only in convoy length.

first half of the convoy the small pressure differences observed are attributed to the different wagon areas exposed to the wind: RILSN wagons are taller (4.28 m vs 4 m) and wider (3 m vs 2.45 m of maximum width), therefore resulting in higher negative pressures. Regarding the different slope of the Δp_{FR} observed in the second part of the train, it can be related to boundary layer development. Indeed, the geometries differ at the leading edge, where RILNS wagons present a pronounced step that increases flow separation, enlarges the local negative pressure peak, and alters boundary layer formation. Finally, two different empty wagon types are considered: an unloaded flatbed (*Train 5*) and an unloaded RGS wagons (*Train 6*). In this case, the TNS curves are markedly different. *Train 5* exhibits the maximum negative pressure at the locomotive, followed by a strong pressure recovery and an almost constant pressure level along the train, with small increments in correspondence of the flatbed wagons. In this case, the pressure reduction is around 74% with respect to the worst-case scenario, namely *Train2*.
Train 6, on the other hand, although unloaded, shows negative peak pressures comparable to those of *Train 3*. This behaviour is attributed to the vertical bars, characteristic of RGS wagons, used to prevent load loss, which disturb the flow field and generate significant pressure variations.

Train number	**Wagon type**	**Min pressure**
Train 1	containers 40 ft	-1321.4 Pa
Train 2	containers HC 40 ft	-1433.2 Pa
Train 3	containers 60 ft	-625.8 Pa
Train 4	RILNS	-816.1 Pa
Train 5	unloaded flatbed	-369.5 Pa
Train 6	unloaded RGS	-569.4 Pa

Table 2: Simulations performed to assess the wagon geometric effects.

4.2 Convoy composition

The effects of the convoy composition are assessed by observing the TNS curves obtained by varying the train length and the inter-vehicle gaps.

4.2.1 Train length

To assess the effects of the train length, three different train configurations, with lengths in the typical range of the Italian freight train fleet, have been investigated. Table 3 summarizes the investigated configurations and their corresponding train lengths. The trains studied share the same locomotive but differ in the number of flatbed wagons attached to the locomotive. *Train 1* consists of a locomotive and 15 flatbed 60 ft wagons loaded with 40 ft containers, resulting in a total length of 318 m, while *Train 7* and *Train 8* consist of 24 and 39 wagons of the same type, resulting in total lengths

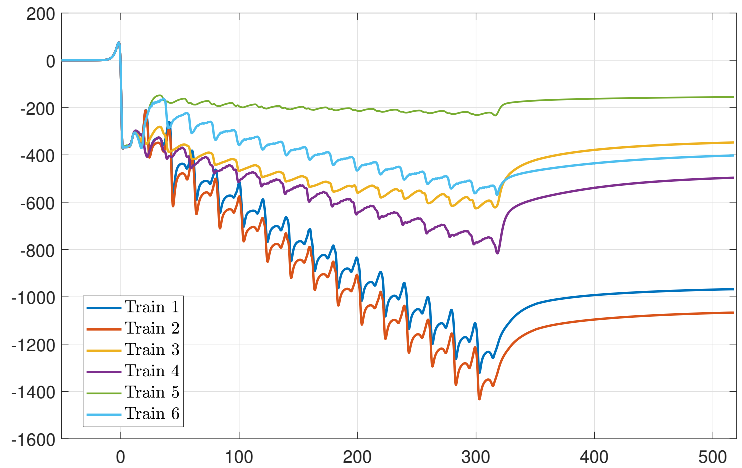

Figure 6: Wagon geometry effects: TNS curves comparison between different wagon types.

of 500 m and 795 m, respectively. The results are displayed in Figure 7a.
Numerical outputs indicate that the convoy length plays a fundamental role in the freight train overpressure phenomenon. As a matter of fact, for the type of train investigated in this study, the pressure minimum decreases almost linearly with increasing train length, reaching minimum values of -1321 Pa for *Train 1*, -2079 Pa for *Train 7*, and -3084 Pa for *Train 8*.

Train number	Train length	Min pressure
Train 1	318 m	-1321.4 Pa
Train 7	500 m	-2079.1 Pa
Train 8	795 m	-3085.0 Pa

Table 3: Simulations performed to assess the train length effect.

4.2.2 Inter-vehicle gaps influence

The effects of inter-vehicle gaps are assessed by comparing simulations of seven trains with the same length, i.e. 318 m, but different loading conditions. Table 4 summarizes the investigated configurations and their corresponding loading conditions.

The results, shown in Figure 7b, highlight the role of inter-wagon gaps as a key parameter affecting the train pressure signature. A first comparison can be made between *Train 1* and *Train 3*. Both trains are fully loaded; however, the former is loaded with 40 ft containers, whereas the latter is loaded with 60 ft containers, resulting in smaller inter-vehicle gaps. In this case, *Train 3* behaves as a more uniform body and exhibits a 52.8% reduction in the pressure peak with respect to *Train 1*.
Different behaviours are observed when the inter-vehicle gaps are increased through

Train number	Convoy loading	Min pressure
Train 1	Train fully loaded with 40 ft containers	-1321.4 Pa
Train 3	Train fully loaded with 60 ft containers	-625.8 Pa
Train 5	Train fully unloaded	-369.5 Pa
Train 9	Train half loaded with 40 ft containers	-994.6 Pa
Train 10	Train half loaded with 60 ft containers	-807.8 Pa
Train 11	Train loaded with 40 ft containers each 3 flatbeds	-865.9 Pa
Train 12	Train loaded with 60 ft containers each 3 flatbeds	-717.4 Pa

Table 4: Simulations performed to assess the inter-vehicle gaps effect.

partially loaded configurations. For the trains loaded with 40 ft containers, namely Train 9 and Train 11, corresponding respectively to a half-loaded configuration and to a configuration with one container every three flatbeds, the larger gaps lead to a reduction of the pressure signature compared to the fully loaded configuration (*Train 1*). Conversely, for the trains loaded with 60 ft containers (*Train 10* and *Train 12*), increasing the gaps results in larger negative pressure peaks compared to the fully loaded configuration (*Train 3*). In this latter case, the most severe condition is observed for the half-loaded configuration, i.e. *Train 11*, whereas the configuration with a container each three flatbeds (*Train 12*) exhibits a less pronounced increase.
These results suggest a complex phenomenon governed by the balance between the negative pressure increase generated at the wagon leading edge, generally more severe in the case of larger gaps, as found by [18], and the subsequent pressure recovery ahead of the following wagon, which also increases with gap size. Consequently, enlarging the inter-vehicle gaps may either improve or worsen the train-tunnel pressure signature depending on the original flow development along the train. In general, for less uniform trains characterised by a continuously redeveloping boundary layer, larger gaps may have a beneficial effect because the increase in pressure recovery exceeds the augmentation of the local pressure variation ahead of the wagon, $\Delta p_{N,w}$. Conversely, for more uniform trains characterised by an almost fully developed boundary layer, increasing the gaps may lead to more severe pressure conditions.

5 Concluding remarks

The pressure signature of freight trains entering a tunnel was investigated in this work. In particular, Train Near-field Signatures (TNS) were analysed using 3D compressible steady-state CFD simulations. The numerical approach reproduces the quasi-steady nature of the problem during train passage inside the tunnel while significantly reducing computational cost compared to sliding mesh methods. The numerical model was validated against full-scale experimental data.
The influence of wagon geometry, train length, and inter-vehicle gaps on the TNS was assessed.
Wagon geometry was found to strongly affect the pressure signature. Comparable

TNS curves were obtained for 40 ft container configurations (e.g. *Train 1* and *Train 2*), which represent the most severe cases. RILNS wagons exhibit a reduction of approximately 40% in the maximum negative pressure peak. For unloaded configurations, flatbed wagons show a pronounced peak at the locomotive, with a pressure reduction of about 74% relative to the most severe case. In contrast, unloaded RGS wagons produce pressure peaks comparable to those of 60 ft container trains, due to flow disturbances induced by the vertical bars.
The effect of inter-vehicle gaps was found to be configuration-dependent. For homogeneous trains with a well-developed boundary layer, larger gaps increase pressure peaks by up to 29%. Conversely, in configurations characterised by already large spacing and thicker boundary layers, further gap enlargement reduces pressure loads, with peak reductions up to 34%.
Finally, train length shows an approximately linear influence on pressure variations. A 1.57-fold increase in train length results in a comparable increase in pressure, while a 2.5-fold increase leads to an approximately 2.3-fold increase.
Future work should extend the range of investigated parameters to capture a broader spectrum of TNS behaviours. In addition, the influence of the relative velocity induced by the train piston effect should be included in the analyses to improve the physical fidelity of the predicted pressure signature.

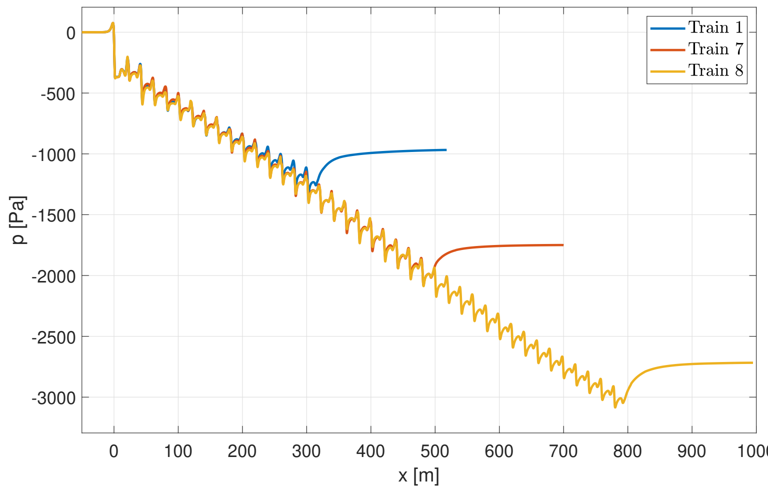

(a) Train length effects: TNS curves comparison between 318 m, 500 m and 795 m trains.

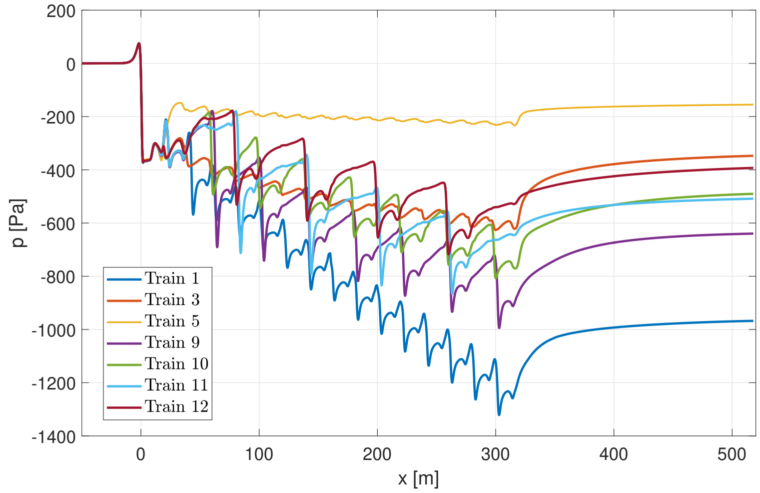

(b) Inter-vehicle gaps effects: comparison between different convoy loading conditions.

Figure 7: Convoy composition effects on TNS curves: train length and inter-wagon gaps.

References

[1] EN 14067-5, "Railway applications — Aerodynamics. Part 5: Requirements and assessment procedures for aerodynamics in tunnels", 2021.

[2] TSI Infrastructures, "COMMISSION REGULATION (EU), No 1299/2014, on the technical specifications for interoperability relating to the 'infrastructure' subsystem of the rail system in the European Union, 2014.

[3] Y.-Y. Ko, C.-H. Chen, I.-T. Hoe, S.-T. Wang, "Field Measurements of Aerodynamic Pressures in Tunnels Induced by High-Speed Trains", Journal of Wind Engineering and Industrial Aerodynamics, 100(1), 19-29, 2012. DOI:10.1016/j.jweia.2011.10.008.

[4] C. Somaschini, T. Argentini, E. Brambilla, D. Rocchi, P. Schito, G. Tomasini, "Full-Scale Experimental Investigation of the Interaction Between Trains and Tunnels", Applied Sciences, 10(20), 7189, 2020. DOI: 10.3390/app10207189.

[5] P. Iliadis, D. Soper, C. Baker, H. Hemida, "Experimental Investigation of the Aerodynamics of a Freight Train Passing Through a Tunnel Using a Moving Model", Proceedings of the Institution of Mechanical Engineers, Part F: Journal of Rail and Rapid Transit, 233(8), 857–868, 2019. DOI: 10.1177/0954409718811736.

[6] J. Niu, Y. Sui, Q. Yu, X. Cao, Y. Yuan, "Aerodynamics of Railway Train/Tunnel System: A Review of Recent Research", Energy and Built Environment, 1(4), 351–375, 2020. DOI: 10.1016/j.enbenv.2020.03.003.

[7] J. Niu, D. Zhou, F. Liu, Y. Yuan, "Effect of Train Length on Fluctuating Aerodynamic Pressure Wave in Tunnels and Method for Determining the Amplitude of Pressure Wave on Trains", Tunnelling and Underground Space Technology, 80, 277–289, 2018. DOI: 10.1016/j.tust.2018.07.031.

[8] J. Du, Q. Fang, X. Zhang, H. Wang, "Aerodynamic Effect Associated with Tunnel Length", KSCE Journal of Civil Engineering, 28(7), 2997–3008, 2024. DOI: 10.1007/s12205-024-1299-6.

[9] A. Baron, M. Mossi, S. Sibilla, "The Alleviation of the Aerodynamic Drag and Wave Effects of High-Speed Trains in Very Long Tunnels", Journal of Wind Engineering and Industrial Aerodynamics, 89(5), 365–401, 2001. DOI: 10.1016/S0167-6105(00)00071-4.

[10] P. Ricco, A. Baron, P. Molteni, "Nature of Pressure Waves Induced by a High-Speed Train Travelling Through a Tunnel", Journal of Wind Engineering and Industrial Aerodynamics, 95(8), 781–808, 2007. DOI: 10.1016/j.jweia.2007.01.008.

[11] C.-R. Chu, S.-Y. Chien, C.-Y. Wang, T.-R. Wu, "Numerical Simulation of Two Trains Intersecting in a Tunnel", Tunnelling and Underground Space Technology, 42, 161–174, 2014. DOI: 10.1016/j.tust.2014.02.013.

[12] J. Du, Q. Fang, X. Zhang, H. Wang, "Comparative Analysis Between Single-Train Passing and Double-Train Intersection in a Tunnel", Journal of Zhejiang University Science A, 25, 429–442, 2024. DOI: 10.1631/jzus.A2300339.

[13] J. Östh, S. Krajnović, "A Study of the Aerodynamics of a Generic Container Freight Wagon Using Large-Eddy Simulation", Journal of Fluids and Structures, 44, 31–51, 2014. DOI: 10.1016/j.jfluidstructs.2013.09.017.

[14] D. Flynn, H. Hemida, D. Soper, C. Baker, "Detached-Eddy Simulation of the Slipstream of an Operational Freight Train", Journal of Wind Engineering and Industrial Aerodynamics, 132, 1–12, 2014. DOI: 10.1016/j.jweia.2014.06.016.

[15] S. Giappino, S. Melzi, G. Tomasini, "High-Speed Freight Trains for Intermodal Transportation: Wind Tunnel Study on the Aerodynamic Coefficients of Con-

tainer Wagons", Journal of Wind Engineering and Industrial Aerodynamics, 175, 111–119, 2018. DOI: 10.1016/j.jweia.2018.01.047.

[16] P. Iliadis, H. Hemida, D. Soper, C. Baker, "Numerical Simulations of the Separated Flow Around a Freight Train Passing Through a Tunnel Using the Sliding Mesh Technique", Proceedings of the Institution of Mechanical Engineers, Part F: Journal of Rail and Rapid Transit, 234(6), 638–654, 2020. DOI: 10.1177/0954409719851421.

[17] Z. Liu, D. Soper, H. Hemida, B. Chen, "A Study of the Influence of Separation Bubbles Around a Generic Freight Train on Pressure Waves Inside Tunnels Using 1D and 3D Numerical Methods", Journal of Wind Engineering and Industrial Aerodynamics, 240, 105461, 2023. DOI: 10.1016/j.jweia.2023.105461.

[18] Z. Liu, D. Soper, H. Hemida, B. Chen, "Numerical Modelling of a Partially Loaded Intermodal Container Freight Train Passing Through a Tunnel", arXiv Preprint, arXiv:2509.09591, 2025. DOI: arXiv:2509.09591.

[19] F. Menter, "Zonal Two Equation k–ω Turbulence Models for Aerodynamic Flows", 23rd Fluid Dynamics, Plasmadynamics, and Lasers Conference, Paper 2906, 1993.

[20] F.R. Menter, "Two-Equation Eddy-Viscosity Turbulence Models for Engineering Applications", AIAA Journal, 32(8), 1598–1605, 1994.

[21] E. Brambilla, P. Schito, C. Somaschini, D. Rocchi, "Virtual Homologation of High-Speed Trains in Railway Tunnels: A New Iterative Numerical Approach for Train-Tunnel Pressure Signature", Proceedings of the Institution of Mechanical Engineers, Part F: Journal of Rail and Rapid Transit, 236(5), 511–531, 2022. DOI: 10.1177/09544097211029164.